An Integrated Force Sensing Interface Enabling Decoupling of Human and Robot Inputs for Physical Human-Robot Collaboration

Nicky Mol[1], Yesica van Binsbergen[1], Mats Kasse[1], Britte Leenards[1], Joris Nankman[1], David A. Abbink[1,2], Luka Peternel[1], and J. Micah Prendergast[1]

2025 International Conference on Advanced Robotics and Mechatronics (ICARM) | 979-8-3315-0307-9/25/$31.00 ©2025 IEEE | DOI: 10.1109/ICARM65671.2025.11293669

***Abstract*— Despite recent advancements in physical human-robot collaboration, measuring and distinguishing between forces applied by humans and robots remains challenging, limiting our understanding of force dynamics during collaboration. Our proposed solution addresses this gap with a low-cost, lightweight design that integrates directly at the robot end-effector level. The interface employs a three-ring mechanical structure with strategically positioned load cells and a Sarrus mechanism to constrain movement to the z-axis only, enabling tool mounting for real-world collaborative tasks such as blending or sanding operations. Validation experiments demonstrate excellent force decoupling capabilities with minimal cross-interference, achieving Weighted Root Mean Squared Errors of 0.14 N for robot-applied forces and 0.08 N for human-applied forces compared to ground truth measurements in steady-state for loads ranging from 0 N up to 23 N. The Maximum Absolute Error in these experiments is 0.33 N, confirming high measurement accuracy. This affordable and integrated solution lowers the threshold for employing decoupled force sensing in collaborative tasks, making it more accessible for investigating force dynamics and developing adaptive control strategies in both research and practical applications of physical human-robot collaboration.**

I. INTRODUCTION

The global industrial landscape is undergoing rapid transformation, driven by complex societal challenges including labor shortages, aging populations, and escalating production demands.Traditional industrial robots have demonstrated significant value in highly repetitive and controlled environments, such as automotive manufacturing. However, industries requiring flexibility—such as repair, maintenance, and flexible manufacturing—present unique challenges that require more adaptive solutions. Jet engine fan blade blending/maintenance, as an example, requires human expertise but may still benefit from robotic assistance (Fig. 1). Recent advancements in robotics have led to the development of collaborative robots, or Cobots [1] enabling physical Human-Robot Collaboration (pHRC) [2] which aims at combining the cognitive capabilities of workers with the physical capabilities of robots [3], fostering a more efficient, effective, and flexible workforce.

Fig. 1: A representative example of collaborative blending during jet engine turbine blade maintenance, where the developed interface can replace the existing tools (green). This use case is part of the BrightSky project.

Despite these advancements, much work remains to be done before Cobots can truly collaborate effectively with humans in physical tasks [4]. To achieve effective physical collaboration, understanding the forces that are at play when physically collaborating with a robot is essential for task performance [2], [5]. Existing research often draws insights from how humans physically interact with each other to better understand these force-based communications [6]. However, studies suggest that physical interaction behaviors are influenced even by awareness that one is collaborating with a robot, rather than another human [7]. This underscores the need for further investigation into how forces during collaboration with robots affect performance.

Untangling the individual robot and human contributions to physical interaction behavior requires accurate estimation or measurement at the point of physical interaction. There are methods that measure robot and human forces individually. A

[1]N. Mol, Y. van Binsbergen, M. Kasse, B. Leenards, J. Nankman, D.A. Abbink, L. Peternel and J.M. Prendergast are with the Department of Cognitive Robotics, Delft University of Technology, 2628 CD Delft, The Netherlands.

[2]D.A. Abbink is with the Department of Sustainable Design Engineering, Delft University of Technology, 2628 CD Delft, The Netherlands.

N. Mol is the corresponding author of this study (e-mail: nicky.mol@tudelft.nl).

The authors would like to thank Dr. Freek G.J. Broeren for advice on methods and mechanisms to constrain motion.

*This work was supported by the BrightSky project, funded by the R&D Mobiliteitsfonds from the Netherlands Enterprise Agency (RVO) and commissioned by the Ministry of Economic Affairs and Climate Policy.

common method to measure robot forces is by equipping the robot with force/torque sensors at the end-effector level [8], [9]. To avoid the costs of such sensors, and the potentially undesirable added mass and dynamics, an alternative is to estimate the forces at the end-effector, either by using model-based disturbance observers [10] or by utilizing the joint torque sensors that are available in many cobots [11], [12]. This is typically less accurate, due to the accumulated noise from the torque sensors and model inaccuracies. Another alternative, applicable only to known deformable surfaces, is to use vision-based force estimation methods [13], [14], which require good lighting conditions and an unobstructed view.

The key problem when only relying on these sensors or estimation methods is that they do not distinguish between human and robot force input. Distinguishing between human and robot forces during task execution is useful for making robots adapt to their human collaborators based on force sensing information [15]. Furthermore, this distinction can enable an effective shared authority between the human and the robot [16], for example, to account for human ergonomics during collaboration [17]. In lab-based experimental setups, external force/torque sensors can be integrated into the task environment to get accurate force readings [18], [19], and when combined with methods stated above, it is potentially possible to distinguish between human and robot input. However, apart from being expensive and lacking flexibility in terms of the task environment, these controlled lab setups are often tailored towards the goal of doing studies and representing abstractions of real-world tasks. However, in real-world scenarios, integrating these sensors into the environment is often not feasible.

Some methods in pHRC aim at estimating the human force indirectly through human effort with biosignals, such as electromyography [20], [21] and electrical impedance tomography [22]. While these estimates on the human side can be effective in controlling and learning various collaborative behaviors, such estimates do not give exact values of the force when it is crucial for task performance. Furthermore, these methods require wearable sensors that are typically difficult to use. Therefore, the existing force sensing interfaces fail to provide a practical solution to measure human and robot forces in a decoupled manner.

To address this gap, we propose a low-cost force sensing interface that enables the decoupling of human and robot input forces and can be directly integrated at the end-effector of cobot manipulators. Our approach leverages a mechanical design that decouples human and robot force components through strategically placed compression and tension load cells. The system is lightweight, modular, and adaptable to various robotic platforms, making it well-suited for dynamic and real-world pHRC applications. Additionally, by integrating force sensing at the end-effector level, the system eliminates the need for external sensors, enabling accurate and flexible force measurements in diverse environments. An additional important feature is that the mechanical interface enables the mounting of tools needed for collaborative task execution, such as a polishing machine for blending operation. To validate the developed system, a controlled experiment has been executed with the goal of showing the decoupling of forces and the accuracy of the measured forces using this affordable integrated design.

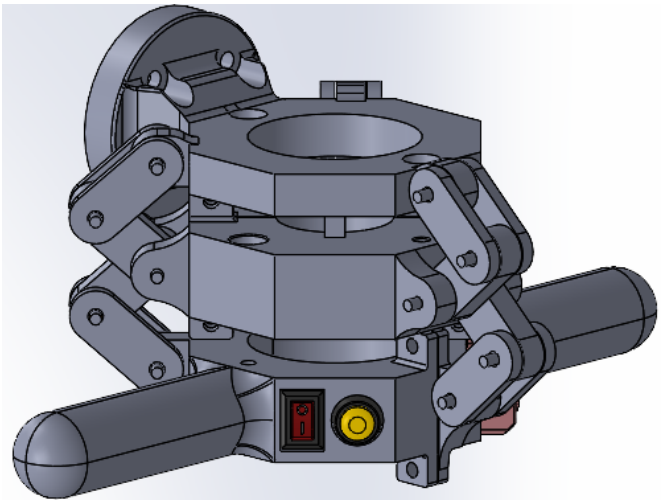

Fig. 2: Interface overview: top ring for robot attachment, bottom ring with handles, and Sarrus mechanism ensuring motion between the rings is constrained to the z-axis only. The three rings feature a central tool mount (e.g., polishing machine). Integrated buttons (left: switch/push; right: scroll wheel/push) that allow for operator control.

II. DESIGN

The development of the integrated force sensing interface was guided by the following design requirements:

- **R1: Decoupling of human and robot force**. The interface must independently measure forces applied by the operator and the robot during physical collaboration.
- **R2: Integration with robotic end-effectors**. The interface must be modular and easily mountable on standard collaborative robot end-effectors, requiring no significant modifications and not relying on any external hardware.
- **R3: Measurement range**. The interface must be able to measure forces up to 150 N in the z-axis of the tool, supporting a broad range of collaborative applications.
- **R4: Measurement resolution**. The resolution of the force measurements must be at least 0.125 N, ensuring fine-grained sensing for accurate control and analysis.
- **R5: Measurement accuracy**. The interface must provide reliable force measurements with an accuracy of $\pm$ 1 N, validated using a secondary F/T sensor.
- **R6: Low cost**. The interface must use affordable components to achieve a cost-effective design, accessible for both research and industrial applications.
- **R7: Lightweight design**. The total weight of the interface must remain below 1 kg to prevent excessive impact on the robot's payload capacity and dynamics.

The final version of the interface design is shown in Fig. 2. The proposed force sensing interface consists of three main components: (1) a mechanical structure consisting of a three-ring configuration that enables force decoupling, (2)

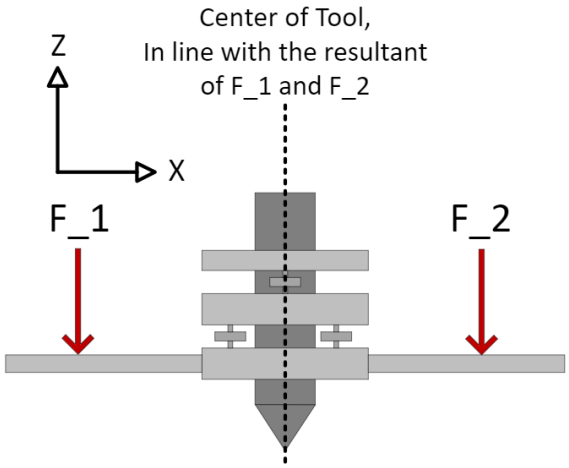

Fig. 3: The center line of the tool is in line with the resultant of forces F_1 and F_2)

a sensing array with strategically positioned load cells, and (3) a constraint mechanism to minimize forces and torques that are not aligned with the direction of measurement in the z-axis.

A. Mechanical Design

The three-ring structure plays a crucial role in the force decoupling and consists of a top ring that interfaces with the robot end-effector, providing a rigid attachment. The bottom ring contains the interface that the operator uses to control the tool, positioned close to the tool-tip of the tool for intuitive and ergonomic operation. The middle ring rigidly holds the tool in place, ensuring accurate force transfer to the sensing array. The middle ring is connected to the top and bottom rings solely through strategically placed load cells. Fig. 3, illustrates the placement of the sensors relative to the forces F_1 and F_2 applied by the operator. Two load cells are positioned symmetrically on the left and right sides of the middle ring near the tool, ensuring that the resultant human force acts along the centerline. This placement minimizes torque and ensures accurate measurements. In addition, the symmetric positioning of these sensors also allows for the estimate of disproportionate loading in the case that one handle is pushed harder than the other.

Robot forces are measured through perpendicularly oriented load cells positioned between the top and middle rings, as can be seen in Fig. 4. The load cells between the top and middle rings compress when a force is applied by the robot, while the load cells between the bottom and middle rings are tensioned when the operator applies a force. Affordable bidirectional load cells are used to ensure compatibility with both tension and compression forces, while minimizing costs.

To ensure that only forces along the z-axis are measured and to minimize the influence of undesired forces and torques during operation, while maintaining a parallel alignment between the rings, a Sarrus mechanism is incorporated into the design [23]. This mechanism is critical for measurement accuracy as it constrains the relative motion of the rings strictly to pure translation along the z-axis. By effectively eliminating unwanted movement in other directions, it ensures that

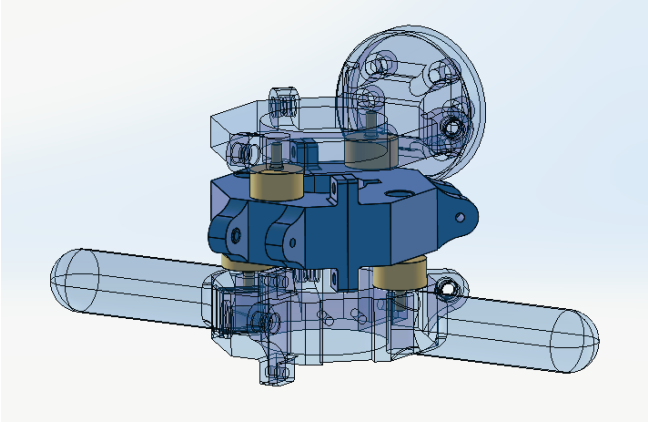

Fig. 4: Force sensing system with sensors (gold cylinders) placed between the rings. Two sensors responsible for measuring robot forces are placed between the top and middle ring, while the two sensors responsible for measuring the human forces are placed between the bottom and middle ring.

the load cells only register the intended force component. Fig. 2 illustrates the Sarrus mechanism, which is constructed from steel rods, ball bearings, and lightweight 3D-printed components, ensuring a balance between structural rigidity and minimal weight. Additionally, the mechanism is pre-tensioned to eliminate slack, which reduces measurement noise and enhances the overall accuracy of the force-sensing system.

B. Electronics Integration

For the purpose of modularity, all necessary electronics are integrated onboard the force decoupling system. As noted, four identical single-axis load cells (A4M7, Qlsensor Co., Bengbu City, China) are used for force sensing for both the robot and the human. The analog signals from these load cells are amplified via four inline amplifiers (HX711, Avia Semiconductor, Xiamen, China). This amplifier includes a 24-bit AD converter and the resulting digital signals are passed to a Teensy 4.0 microcontroller at 10Hz. Three user-programmable buttons, including a rocker switch, push button and scroller button are integrated into the handles of the system to enable ease of use during interaction. Power and signal connections to the microcontroller and amplifiers are passed via a single USB cable, enabling serial communication between the host computer and the force decoupling system. Forces read by the microcontroller are passed to the host computer at 10Hz and button presses are read as either interrupts (in the case of the rocker switch and push button) or as an analog signal (in the case of the scroller). All electronics hardware and connecting cables are housed cleanly within the mock tool.

III. EXPERIMENTAL VALIDATION

To evaluate the performance of the proposed force sensing interface, a validation experiment was conducted. The experimental setup consists of a Cartesian impedance-controlled KUKA LBR14 iiwa 7-DOF manipulator, which is controlled using the KUKA Fast Robot Interface (FRI), running at 1 kHz [24], equipped with the proposed force sensing interface

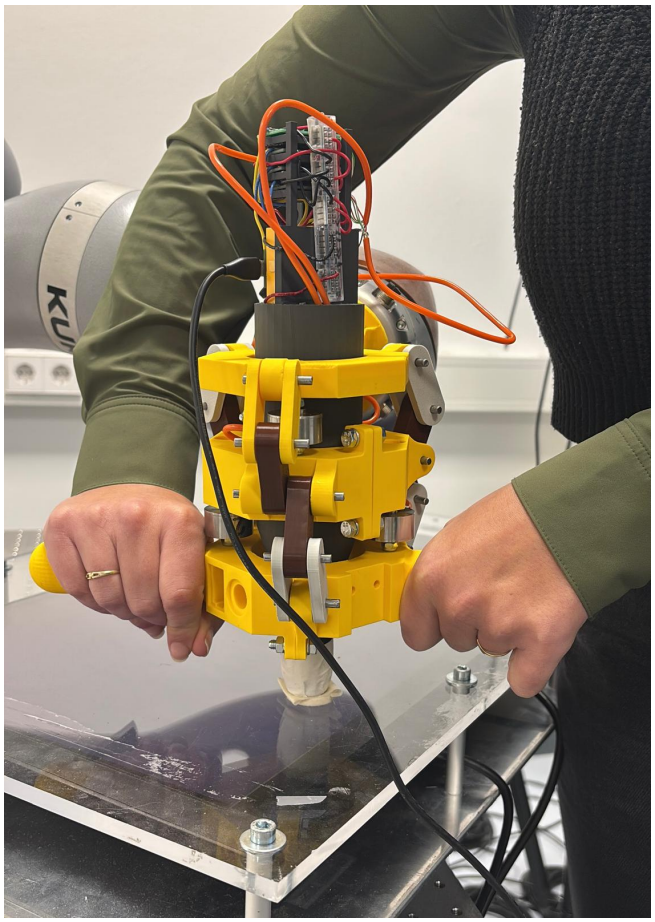

Fig. 5: Experimental setup showing the proposed force sensing interface (yellow) attached to a Kuka LBR14 iiwa collaborative robotic arm. Below there is a sensorised screen that can measure forces as applied by the tooltip, which is used to validate the results.

at its end-effector (Fig. 5). A 23.8-inch FHD Dell monitor is used to display the blending task and is encased in a box with a plexiglass surface, which is connected to a 6-DOF SCHUNK force/torque sensor (Schunk FTN-Delta SI-330-30) mounted beneath the workpiece which serves as ground truth measurement for validation purposes which has been calibrated using known weights. The Cartesian impedance controller has been written in the C++ programming language and is based on the work by Christian Ott [25]. To be able to operate within the ROS framework, the controller was implemented using ROS control [26]. The load cells used in the interface, showed inconsistent results using factory calibration, so additional calibration of the load cells was conducted.

1) Load Cell Calibration: Prior to experiments, each load cell was individually calibrated using known weights to establish calibration factors. For human force sensors, calibration involved symmetrically hanging known weights (1 kg, 2 kg, and 3 kg) on the handles (Fig. 6a). Robot force sensors were calibrated by placing known weights (1 kg, 2 kg, and 5 kg) on the tooltip (Fig. 6b). Each weight test was repeated four times for every load cell, and the averaged results were used to determine the final calibration factors shown in Table I.

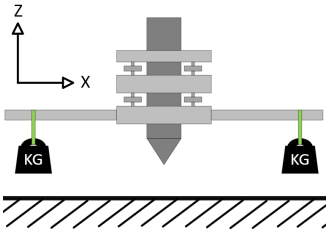

(a) Human force is calibrated by symmetrically hanging known weights on the handles.

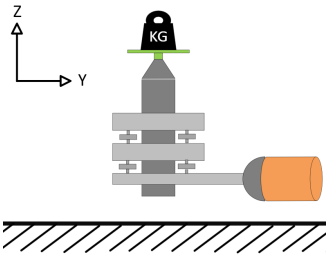

(b) Robot force is calibrated by placing known weights on the tooltip.

Fig. 6: Setups for human and robot force calibration.

TABLE I: CALIBRATION FACTORS

	Calibration factor
Cell 1 human force	−52.43
Cell 2 human force	−53.87
Cell 3 robot force	54.47
Cell 4 robot force	56.78
Schunk F/T sensor	0.20

A. *Validation Experiment*

The validation experiment aimed to demonstrate the system's ability to decouple human and robot forces and measure them accurately against a ground truth in steady-state. The experiment consisted of two tests:

- **Test 1 - Human force only:** Step-wise increase in human force without robot input force
- **Test 2 - Robot force only:** Step-wise increase in robot force without human input force

During the tests, the robot arm is controlled to exert a series of predefined forces in the z-direction on the 6-DOF sensor. The force in the task frame was controlled at the robot joint-torque level as:

$$\boldsymbol{\tau} = \boldsymbol{M}(\boldsymbol{q})\ddot{\boldsymbol{q}} + \boldsymbol{C}(\boldsymbol{q}, \dot{\boldsymbol{q}})\dot{\boldsymbol{q}} + \boldsymbol{g}(\boldsymbol{q}) + \boldsymbol{J}^T \boldsymbol{f}, \tag{1}$$

where $\boldsymbol{\tau}$ are joint torques, $\boldsymbol{M}$ the mass matrix, $\boldsymbol{C}$ the centrifugal and Coriolis matrix, $\boldsymbol{g}$ the gravity vector, $\boldsymbol{J}$ the robot Jacobian matrix, $\boldsymbol{q}$ the joint angles and $\boldsymbol{f}$ being the interaction force/torque that is acting on the environment defined as:

$$\boldsymbol{f} = \boldsymbol{K}(\boldsymbol{x}_a - \boldsymbol{x}_d) + \boldsymbol{D}(\dot{\boldsymbol{x}}_a - \dot{\boldsymbol{x}}_d) + \boldsymbol{S}_f \boldsymbol{f}_d, \tag{2}$$

where $\boldsymbol{K}$ and $\boldsymbol{D}$, being the diagonal stiffness and damping matrices in Cartesian space, $\boldsymbol{x}_a$ and $\boldsymbol{x}_d$ being the actual and desired robot end-effector pose in Cartesian space, $\boldsymbol{S}_f$ a diagonal matrix used for selecting the axis in which the desired force is applied and $\boldsymbol{f}_d$ the desired force, both in

Cartesian space. The robot and the interface are gravity compensated. The diagonal stiffness matrix $\boldsymbol{K}$ was chosen such that the translational stiffness of 3000 N/m acted in the x-axis and y-axis, leaving the z-axis with a stiffness of 0 N/m. The rotational stiffness of the stiffness matrix $\boldsymbol{K}$ was set to 70 N/rad for rotations around all axes. All diagonal elements of the damping matrix $\boldsymbol{D}$ were set for a critically damped system: $\boldsymbol{D} = 2\zeta\sqrt{\boldsymbol{K}}$, with $\zeta = 0.7$. The diagonal selection matrix $\boldsymbol{S}_f$ was chosen to only allow desired forces $\boldsymbol{f}_d$ in the z-direction.

For validating the accuracy, the Weighted Root Mean Squared Error (W-RMSE) is calculated by comparing the measured human input force and the reference force in the first test scenario and the measured robot input force and the reference force in the second test scenario. The RMSE_j over a steady-state region j is calculated as follows:

$$\text{RMSE}_j = \sqrt{\frac{1}{n}\sum_{i=1}^{n}(f_{h/r,z,i} - f_{ref,z,i})^2} \tag{3}$$

Where $f_{h/r,z,i}$ is either the measured human input force or robot input force in z-direction, $f_{ref,z,i}$ is the measured reference force in z-direction, and n is the number of data points in the steady-state region. The Weighted RMSE is calculated as follows:

$$\text{W-RMSE} = \sum_{j=1}^{m} w_j \cdot \text{RMSE}_j \tag{4}$$

Where m is the number of steady-state regions, w_j is the weight for region j based on its duration as part of the total duration of steady-state regions, and RMSEj is the RMSE calculated for steady-state region j. Moreover, to fully characterize the system's accuracy, the Maximum Absolute Error (MAE) is reported, showing the worst-case deviation.

The results of these tests are shown in Fig. 7 and Fig. 8. The results demonstrate effective force decoupling across both scenarios. When a force is applied by the robot while no human force is exerted, the measured human input force remains close to zero, indicating minimal cross-interference. However, when a human force is applied while the robot is not exerting any forces, a small but noticeable response is observed in the robot force sensors.

This residual coupling effect likely arises due to the imperfect gravity compensation of the robotic system. Although the robot controller compensates for gravity, minor dynamic effects—such as unmodeled joint friction, sensor noise, or slight inaccuracies in the compensation model—can introduce imperfect compensation. Since the load cells physically connect the rings, and the robot is rigidly attached to the upper ring, any unintended motion of the lower ring (caused by the human input) can induce a slight contraction or expansion of the upper ring when running into the uncompensated dynamics of the robot. This effect is particularly noticeable during the transition phases, as denoted by the gray regions in Fig. 7. In the steady-state regions, there is also a small offset visible in the robot force, which can be explained by

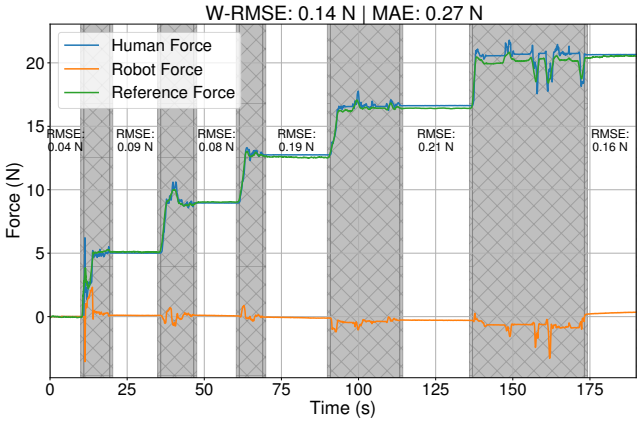

Fig. 7: Force measurements over time showing human input force (blue), robot input force (orange), and reference force (green). Human input forces are incrementally increased stepwise, while providing no robot force input. The grey regions indicate transition behavior, while the white regions indicate steady-state behavior, each showing its individual RMSE between the human input force and the reference force. The average RMSE across the 6 steady-state regions is: 0.13 N, while the MAE is: 0.27 N.

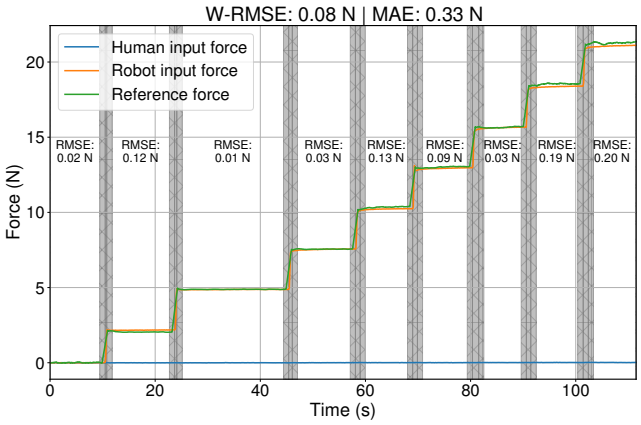

Fig. 8: Force measurements over time showing human input force (blue), robot input force (orange), and reference force (green). Robot input forces are incrementally increased stepwise, while providing no human force input. The grey regions indicate transition behavior, while the white regions indicate steady-state behavior, showing each their individual RMSE between the robot input force and the reference force. The average RMSE across the 9 steady-state regions is: 0.09 N, while the MAE is: 0.33 N

small rotational offsets due to uneven load distribution when applying the weights to the human input handlebars.

The results demonstrate strong agreement between the measured forces from the proposed sensing interface and the reference SCHUNK force/torque sensor. Across all steady-state regions, the measured forces closely follow the ground truth values, confirming the system's high accuracy. The weighted RMSE (W-RMSE), computed over all steady-state regions, is 0.14 N for robot-applied forces and 0.08 N for human-applied forces, indicating minimal deviation from the reference sensor. Furthermore, the MAE remains low with values of 0.27 N and 0.33 N for test 1 and test 2 scenarios, respectively.

IV. CONCLUSION

This paper presented the development and validation of an integrated force-sensing interface for physical human-robot

collaboration that enables decoupled force measurements for both human and robot. The experimental results demonstrate that the proposed system indeed successfully meets the initial design requirements while offering a practical solution for measuring decoupled forces in steady-state.

- **R1:** The interface effectively decouples human and robot forces in the z-axis during physical interaction, as is validated through validation experiments.
- **R2:** The system's modular design enables straightforward integration with collaborative robot end-effectors, as demonstrated through successful implementation on a KUKA LBR14 iiwa manipulator.
- **R3, R4, R5:** The technical specifications (R3, R4) are met by the choice of load cells. The RMSE values across different testing conditions (ranging from 0.01 N to 0.21 N) as well as the MAE (max. 0.33 N), demonstrate measurement accuracy well within the specified requirement of ± 1 N (R5).
- **R6, R7:** The use of affordable load cells and 3D-printed components keeps the total cost low (dependent on the use of materials, but for this specific validation setup approximately €200,-) (R6), while the lightweight design–incorporating the Sarrus mechanism and strategic sensor placement–maintains a total weight well below 1 kg (again dependent on the use of materials, but in our case: 0.89 kg) (R7).

The system's ability to distinguish between human and robot forces enables research into understanding the forces that are at play when physically collaborating with a robot. Moreover, it allows for more sophisticated control strategies, robot learning and opens new possibilities for adaptive collaborative behaviors. Limitations of the current design include its restriction to z-axis force measurement and its validation primarily under steady-state conditions.

REFERENCES

[1] J. E. Colgate, W. Wannasuphoprasit, and M. A. Peshkin, "Cobots: Robots for collaboration with human operators," in *Proc. ASME Int. Mech. Eng. Congr. Expo.*, vol. 15281, Nov. 1996, pp. 433–439.

[2] A. Ajoudani, A. M. Zanchettin, S. Ivaldi, A. Albu-Schäffer, K. Kosuge, and O. Khatib, "Progress and prospects of the human–robot collaboration," *Auton. Robots*, vol. 42, no. 5, pp. 957–975, Jun. 2018.

[3] P. M. Fitts, Ed., *Human engineering for an effective air-navigation and traffic-control system*. Oxford, England: Nat. Res. Counc., Mar. 1951.

[4] J. E. Michaelis, A. Siebert-Evenstone, D. W. Shaffer, and B. Mutlu, "Collaborative or simply uncaged? Understanding human-cobot interactions in automation," in *Proc. CHI Conf. Human Factors Comp. Syst.*, Apr. 2020, pp. 1–12.

[5] Y. Li, A. Sena, Z. Wang, X. Xing, J. Babič, E. van Asseldonk, and E. Burdet, "A review on interaction control for contact robots through intent detection," *Prog. Biomed. Eng.*, vol. 4, no. 3, p. 032004, Aug. 2022.

[6] E. Noohi, M. Žefran, and J. L. Patton, "A model for human–human collaborative object manipulation and its application to human–robot interaction," *IEEE Trans. Robot.*, vol. 32, no. 4, pp. 880–896, Aug. 2016.

[7] K. B. Reed and M. A. Peshkin, "Physical collaboration of human-human and human-robot teams," *IEEE Trans. Haptics*, vol. 1, no. 2, pp. 108–120, Dec. 2008.

[8] L. Roveda, N. Pedrocchi, M. Beschi, and L. M. Tosatti, "High-accuracy robotized industrial assembly task control schema with force overshoots avoidance," *Control Eng. Pract.*, vol. 71, pp. 142–153, Feb. 2018.

[9] K. Haninger, C. Hegeler, and L. Peternel, "Model predictive impedance control with Gaussian processes for human and environment interaction," *Robot. Auton. Syst.*, vol. 165, p. 104431, Jul. 2023.

[10] M. Iskandar, O. Eiberger, A. Albu-Schäffer, A. De Luca, and A. Dietrich, "Collision detection, identification, and localization on the dlr sara robot with sensing redundancy," in *Proc. IEEE Int. Conf. Robot. Autom. (ICRA)*, Jun. 2021, pp. 3111–3117.

[11] A. Albu-Schäffer, S. Haddadin, C. Ott, A. Stemmer, T. Wimböck, and G. Hirzinger, "The dlr lightweight robot: design and control concepts for robots in human environments," *Ind. Robot.*, vol. 34, no. 5, pp. 376–385, Aug. 2007.

[12] S. Haddadin, "The franka emika robot: A standard platform in robotics research," *IEEE Robot. Autom. Mag.*, Dec. 2024.

[13] W. Hwang and S.-C. Lim, "Inferring interaction force from visual information without using physical force sensors," *Sensors*, vol. 17, no. 11, p. 2455, Oct. 2017.

[14] A. Petit, F. Ficuciello, G. A. Fontanelli, L. Villani, and B. Siciliano, "Using physical modeling and rgb-d registration for contact force sensing on deformable objects," in *Proc. Int. Conf. Informat. Control, Autom. Robot. (ICINCO)*, vol. 2, Jul. 2017, pp. 24–33.

[15] Y. M. Hamad, Y. Aydin, and C. Basdogan, "Adaptive human force scaling via admittance control for physical human-robot interaction," *IEEE Trans. Haptics*, vol. 14, no. 4, pp. 750–761, Oct. 2021.

[16] M. Selvaggio, M. Cognetti, S. Nikolaidis, S. Ivaldi, and B. Siciliano, "Autonomy in physical human-robot interaction: a brief survey," *IEEE Robot. Autom. Lett.*, vol. 6, no. 4, pp. 7989–7996, Oct. 2021.

[17] Á. G. Andrés, N. Beckers, D. A. Abbink, and L. Peternel, "Arbitration of authority in physical human-robot collaboration with combined preventive and reactive fatigue management," in *Proc. IEEE RAS/EMBS Int. Conf. Biomed. Robot. Biomechatronics (BioRob)*, Nov. 2022, pp. 1–6.

[18] L. Peternel, L. Rozo, D. Caldwell, and A. Ajoudani, "A method for derivation of robot task-frame control authority from repeated sensory observations," *IEEE Robot. Autom. Lett.*, vol. 2, no. 2, pp. 719–726, Jan. 2017.

[19] N. Mol, J. M. Prendergast, D. A. Abbink, and L. Peternel, "Fitts' list revisited: An empirical study on function allocation in a two-agent physical human-robot collaborative position/force task," *arXiv:2505.04722*, 2025.

[20] C. Zeng, C. Yang, H. Cheng, Y. Li, and S.-L. Dai, "Simultaneously encoding movement and semg-based stiffness for robotic skill learning," *IEEE Trans. Ind. Informat.*, vol. 17, no. 2, pp. 1244–1252, Apr. 2020.

[21] L. Vianello, S. Ivaldi, A. Aubry, and L. Peternel, "The effects of role transitions and adaptation in human–cobot collaboration," *J. Intell. Manuf.*, vol. 35, no. 5, pp. 2005–2019, Jun. 2024.

[22] E. Zheng, Y. Li, Q. Wang, and H. Qiao, "Toward a human-machine interface based on electrical impedance tomography for robotic manipulator control," in *Proc. IEEE/RSJ Int. Conf. Intell. Robot. Syst. (IROS)*, Jan. 2019, pp. 2768–2774.

[23] X. Song, H. Guo, Z. Deng, R. Liu, and B. Li, "Mobility analysis of a family of one-dimensional deployable mechanisms based on sarrus mechanism," in *Proc. IEEE Int. Conf. Mechatronics Autom.*, Aug. 2016, pp. 2265–2271.

[24] R. Bischoff, J. Kurth, G. Schreiber, R. Koeppe, A. Albu-Schäffer, A. Beyer, O. Eiberger, S. Haddadin, A. Stemmer, G. Grunwald *et al.*, "The kuka-dlr lightweight robot arm-a new reference platform for robotics research and manufacturing," in *Proc. Int. Symp. Robot. (ISR)*, Jun. 2010, pp. 1–8.

[25] C. Ott, *Cartesian Impedance Control of Redundant and Flexible-Joint Robots*, 1st ed. New York, NY: Springer, 2008.

[26] S. Chitta, E. Marder-Eppstein, W. Meeussen, V. Pradeep, A. R. Tsouroukdissian, J. Bohren, D. Coleman, B. Magyar, G. Raiola, M. Lüdtke *et al.*, "ros_control: A generic and simple control framework for ros," *J. Open Source Softw.*, vol. 2, no. 20, pp. 456–456, Dec. 2017.